

# Improving the Exploration of High Dimensional Free Energy Landscape by a Combination of Temperature Accelerated Sliced Sampling and Parallel Biasing

Abhinav Gupta, Shivani Verma, and Nisanth N. Nair\*

*Department of Chemistry*

*Indian Institute of Technology Kanpur, 208016 Kanpur, India*

E-mail: nnair@iitk.ac.in

## Abstract

Biased sampling methods such as the Temperature Accelerated Sliced Sampling (TASS), which can explore high dimensional collective variable (CV) space, is of great interest in free energy calculations. Such methods can efficiently sample configurational space even when a large number of CVs for biasing are used while many conventional methods are limited to two or three CVs. In this paper, we propose a modification to the TASS method, called Parallel Bias TASS or PBTASS, wherein a multidimensional parallel metadynamics bias is incorporated on a selected set of CVs. The corresponding time-dependent reweighting equations are derived, and the method is benchmarked. In particular, we compare the accuracy and efficiency of PBTASS with various methods viz. standard TASS, Temperature Accelerated Molecular Dynamics/driven-Adiabatic Free Energy Dynamics, and Parallel Bias Metadynamics. We demonstrate the capability of the PBTASS method by reconstructing the eight-dimensional free energy surface of alanine pentapeptide *in vacuo* from a 25 ns long trajectory. Free energy barriers and free energies of high energy saddle points on the high dimensional free energy landscape of this system are reported.

## 1 Introduction

Computational modeling of transitions from one metastable state to another on a free energy basin is of great interest in molecular simulations. Such simulations are crucial in predicting the mechanism, kinetics, and thermodynamics of chemical reactions and physical transformations. Often, the time-scale at which transitions occur among the metastable states is orders of magnitude larger than the period of bond vibrations in molecules. Thus such transitions are classified as rare-events in molecular simulations. Several enhanced sampling methods have been developed to accelerate such rare-events

in molecular dynamics (MD) simulations.<sup>1-8</sup>

A typical approach to monitor the transitions among the metastable states is by looking at the progress along specific order parameters. The free energies computed along the order parameters can be used to calculate rates of the physio-chemical processes of interest.<sup>8</sup> In this spirit, collective variables (CVs) based enhanced sampling methods are proposed.<sup>6</sup> In these methods, CVs,  $\mathbf{s}(\mathbf{R})$ , which are functions of atomic coordinates  $\mathbf{R}$ , are considered and the quantity of interest is the Helmholtz free energy as a function of  $\mathbf{s}$ , given by,

$$F(\mathbf{s}) = -k_B T \ln P(\mathbf{s}).$$

Here,  $k_B$  is the Boltzmann constant,  $T$  is the temperature of the system, and  $\mathbf{s} \equiv (s_1, \dots, s_n)$  is a vector in the CV-space. The probability distribution,  $P(\mathbf{s})$ , is defined as

$$P(\mathbf{s}') = \left\langle \prod_i^n \delta(s_i(\mathbf{R}) - s'_i) \right\rangle$$

and can be calculated using a normalized histogram of  $\mathbf{s}$  obtained from a canonical ensemble MD trajectory. Enhanced sampling of CVs can be achieved by adding external bias potentials. In umbrella sampling<sup>9,10</sup> (US), a harmonic bias

$$W_h^b(s) = \frac{\kappa_h}{2} (s(\mathbf{R}) - \zeta_h)^2, \quad h = 1, \dots, M, \quad (1)$$

is added to the system, where  $\kappa_h$  is the force constant parameter and  $\zeta_h$  is the mean position of the applied harmonic bias. Once the biased distributions centered at different regions in CV-space,  $P_h^b(s)$ ,  $h = 1, \dots, M$ , are obtained, they are reweighted and combined using the Weighted Histogram Analysis Method (WHAM).<sup>11,12</sup> In WHAM,

the following equations are solved in a self-consistent (iterative) manner,

$$P(s) = \frac{\sum_{h=1}^M n_h P_h^b(s)}{\sum_{h=1}^M n_h \exp[\beta f_h] \exp[-\beta W_h(s)]} \quad (2)$$

where  $f_h$  is computed at every step using  $P(s)$  computed from the previous iteration as,

$$\exp(-\beta f_h) = \int ds \exp[-\beta W_h(s)] P(s) .$$

Here,  $n_h$  is the number of frames in the  $h^{\text{th}}$  umbrella window. Often, the bias  $W_h$  is one-dimensional, and seldom two-dimensional. The advantage of the US method is that a controlled sampling is achievable by the nature of the restraining bias potential. However, while dealing with large systems with several soft-modes, free energy convergence can be very slow, which can be attributed to the inadequate sampling of orthogonal coordinates.<sup>7,8</sup>

In metadynamics (MTD)<sup>13,14</sup> a time-dependent bias,  $V^b(\mathbf{s}, t)$ , is added to the potential,

$$V^b(\mathbf{s}, t) = \sum_{\tau < t} w(\tau) \exp \left[ -\frac{(\mathbf{s}(\mathbf{R}, t) - \mathbf{s}_\tau)^2}{2(\delta s)^2} \right] \quad (3)$$

where  $\tau$  runs over all the time-steps for which the metadynamics bias was updated by augmenting a Gaussian centered at  $\mathbf{s}_\tau \equiv \mathbf{s}(\mathbf{R}; \tau)$ . Here,  $\delta s$  and  $w(\tau)$  are width and height parameters, respectively. In the conventional MTD approach,  $w(\tau)$  is taken as a constant,  $w(\tau) = w(0)$ , while in the well-tempered version of MTD,<sup>15</sup>  $w(\tau)$  is calculated as

$$w(\tau) = w(0) \exp \left[ -\frac{V^b(\mathbf{s}, t)}{k_B \Delta T} \right] . \quad (4)$$

Here  $w(0)$  is the initial height of the Gaussian function, and  $V^b(\mathbf{s}, t)$  is the bias at time  $t$ .

Here  $\Delta T$  is a parameter which controls the bias added at any time  $\tau$  depending on the overall bias at  $\mathbf{s}(\tau)$ . The self-guiding nature of MTD makes it very efficient in studying complex chemical reactions and transformations. The method is widely used and excellent reviews are available.<sup>16–25</sup> However, the efficiency of the method decreases with the dimensionality of the CV-space. Thus the method is largely employed for problems where the dimensionality of the CV-space is not beyond three. Like in the case of the US method, slow convergence of free energy can be encountered when there is inadequate acceleration of (hidden) orthogonal coordinates.<sup>7,23</sup>

In order to overcome the problems due to insufficient sampling of transverse coordinates, the enhanced sampling methods must have the ability to accommodate a large number of CVs. Most importantly, the performance of such methods should not deplete in an exponential manner on increasing the dimensionality of the CV-space. Further, the method should permit the system to exhaustively transverse through relevant regions of a high dimensional CV-space and quickly provide a reliable estimate of the underlying free energy. The bias-exchange MTD (BEMTD)<sup>26,27</sup> approach was put forward to achieve this within the MTD framework. Here a certain number of replicas of the system are first created, and within each replica, a different set of CVs are enhanced sampled by low dimensional MTD bias. Further, exchanges between replicas are attempted using the Metropolis-Hastings scheme. The method is widely used to study complex biological systems. For a review of the technique and its applications, readers are directed to Ref.<sup>7</sup> One of the major drawbacks of this method is that its performance decreases when the distributions of replicas are poorly overlapping, thereby diminishing the exchange probability.

In a similar spirit, Pfaendtner and Bonomi have proposed an alternative MTD approach called Parallel Bias MTD<sup>28</sup> (PBMTD). This method uses a single replica, while many low dimensional biases are applied on a set of CVs to enable extensive sampling

of a high dimensional CV-space. The technique uses a time-dependent bias potential of the form,

$$V^{\text{pb}}(s_1, \dots, s_n, t) = -\frac{1}{\beta} \ln \sum_i^n \exp \left[ -\beta V_i^{\text{b}}(s_i, t) \right] , \quad (5)$$

where  $\beta = (k_{\text{B}}T)^{-1}$  and  $V_i^{\text{b}}(s_i, t)$  is given by Equation (3). Further, the height of the Gaussian bias along a dimension is modified based on the feedback from other dimensions, as

$$w_i(\tau) = w_i(0) \exp \left[ -\frac{V_i^{\text{b}}(s_i, t)}{k_{\text{B}}\Delta T} \right] P_i(s_i) \quad (6)$$

where

$$P_i(s_i) = \frac{\exp \left[ -\beta V_i^{\text{b}}(s_i, t) \right]}{\sum_j^n \exp \left[ -\beta V_j^{\text{b}}(s_j, t) \right]} , \text{ and } i = 1, \dots, n .$$

Here  $P_i(s_i)$  is a feedback function to control the Gaussian height based on the bias deposited along other CVs. The free energy along a CV  $s_i$  can then be calculated as,

$$F_i(s_i) = -\gamma V_i^{\text{b}}(s_i, t \rightarrow \infty) \quad (7)$$

where  $\gamma = (T + \Delta T)/\Delta T$ . This method is a significant improvement over the conventional MTD approach. However, very low values of  $P_i$  with increasing dimensionality can lead to insignificant filling rate. This problem can be addressed to some extent by selectively grouping the CVs.<sup>29</sup> The method is applied to a wide spectrum of complex chemical and biological problems; See Refs<sup>30–34</sup> and references in Ref.<sup>7</sup>

Several other attempts to improve the sampling using a MTD-like bias have been also put forward lately.<sup>25,35–38</sup>

Temperature accelerated molecular dynamics/driven-adiabatic free energy dynam-

ics<sup>2,39,40</sup> is a powerful approach for exploring high dimensional free energy landscapes.<sup>41,42</sup> Hereafter we will denote this method as TAMMD. Accelerated diffusion of the system in the CV-space is achieved in this method by increasing the temperature of the fictitious degrees of freedom that are restrained to the CVs. TAMMD employs the extended Lagrangian,

$$\mathcal{L}_{\text{TAMMD}}(\mathbf{R}, \dot{\mathbf{R}}, \mathbf{z}, \dot{\mathbf{z}}) = \mathcal{L}_0(\mathbf{R}, \dot{\mathbf{R}}) + \sum_{i=1}^n \frac{1}{2} \mu_i \dot{\mathbf{z}}_i^2 - \sum_{i=1}^n \frac{k_i}{2} (s_i(\mathbf{R}) - z_i)^2$$

where  $\mathcal{L}_0$  is the Lagrangian of the physical system,  $\{z_i\}$  is the set of  $n$  fictitious variables corresponding to  $n$  CVs  $\{s_i(\mathbf{R})\}$ ,  $\mu_i$  is the mass of the auxiliary variable  $z_i$ , and  $k_i$  is the harmonic spring constant in the potential that restrains the motion of  $z_i$  and  $s_i$ . Auxiliary variables are set to a high temperature  $\tilde{T}$ , which is much higher than the temperature  $T$  of the physical system. The parameters  $\{\mu_i\}$  and  $\{k_i\}$  are chosen in such a way that the adiabatic separation between the  $\{s_i\}$  and  $\{z_i\}$  degrees of freedom is maintained. Separate thermostats are used to maintain the temperature of the physical system and the extended system. Free energy surface  $F(\mathbf{z})$  can be computed from the probability distribution of the auxiliary variables  $\tilde{P}(\mathbf{z})$  as,

$$F(\mathbf{z}) = -k_B \tilde{T} \ln \tilde{P}(\mathbf{z}) \quad (8)$$

and is a good estimator for the underlying free energy surface  $F(\mathbf{s})$  along the physical coordinates at temperature  $T$ .<sup>2</sup> To further improve the efficiency of this method, a variant of the approach, called Unified Free Energy Dynamics (UFED), was proposed by Tuckerman and co-workers.<sup>43</sup> For a review of TAMMD and related methods, see Refs.<sup>7,8</sup>

To introduce a more controlled exploration of high dimensional free energy surfaces, Temperature Accelerated Sliced Sampling (TASS) approach was introduced.<sup>44</sup> This method is built on the TAMMD Lagrangian wherein a combination of US and MTD

biases are applied on a selected set of CVs. The Lagrangian used in TASS is,

$$\mathcal{L}_{\text{TASS}}(\mathbf{R}, \dot{\mathbf{R}}, \mathbf{z}, \dot{\mathbf{z}}) = \mathcal{L}_{\text{TAMD}}(\mathbf{R}, \dot{\mathbf{R}}, \mathbf{z}, \dot{\mathbf{z}}) - \frac{1}{2}\kappa_h (z_1 - \zeta_h)^2 - V^b(\bar{\mathbf{z}}, t) , \quad h = 1, \dots, M. \quad (9)$$

Here US bias is applied along the auxiliary variable  $z_1$ , and such  $M$  different biases centered at  $\zeta_1, \dots, \zeta_M$  are taken. The restraining force constant of the US bias centered at  $\zeta_h$  is  $\kappa_h$ . The metadynamics bias  $V^b(\bar{\mathbf{z}})$  acting on a subset of the auxiliary space  $\bar{\mathbf{z}} \equiv (z_2, \dots, z_m)$ , with  $m \leq n$  can be optionally considered as well. The probability distributions of auxiliary variables obtained with different biases are then reweighted and combined to get the full high dimensional free energy landscape.<sup>7,44</sup> Other than the benefit of achieving a controlled sampling along  $s_1$ , TASS provides flexibility in selecting different transverse CVs depending on the window  $h$ . Further, a large number of orthogonal CVs can be chosen by virtue of the temperature acceleration of  $\mathbf{z}$ . Different TASS windows can run in parallel, making the computations very efficient. Each window samples a high dimensional slice of the free energy landscape, thereby an exhaustive exploration is achieved through the divide-and-conquer strategy inherent to the TASS method. It was observed that TASS could obtain a quick convergence in free energy barriers.<sup>44–49</sup> For a review of the method, see Refs.<sup>7,8</sup>

In the earlier applications of TASS, only a one-dimensional MTD bias was used. Increasing the dimensionality of the MTD bias decreases the performance of the method. In this work, we propose a modified TASS approach, called Parallel Bias TASS (PB-TASS), to improve the efficiency of the method further. This is accomplished by replacing the one-dimensional MTD bias used in the conventional TASS method by a high dimensional PBMTD bias. A modified TASS reweighting scheme, accounting the PBMTD bias, has been put forward. The method is benchmarked for its accuracy and efficiency. Finally, PBTASS is used to explore the eight-dimensional free energy land-



scape of alanine pentapeptide (*in vacuo*).

## 2 Theory

We introduce the Parallel Bias TASS (or PBTASS) method that incorporates PBMTD bias within TASS as follows:

$$\mathcal{L}_{\text{PBTASS},h}(\mathbf{R}, \dot{\mathbf{R}}, \mathbf{z}, \dot{\mathbf{z}}) = \mathcal{L}_{\text{TAMD}}(\mathbf{R}, \dot{\mathbf{R}}, \mathbf{z}, \dot{\mathbf{z}}) - \frac{1}{2}\kappa_h (z_1 - \zeta_h)^2 - V^{\text{pb}}(\bar{\mathbf{z}}, t) , \quad h = 1, \dots, M. \quad (10)$$

The PBMTD bias  $V^{\text{pb}}(\bar{\mathbf{z}}, t)$ , as given by Equation (5), is applied on a subset of auxiliary variables  $\bar{\mathbf{z}} \equiv (z_2, \dots, z_m)$ , with  $m \leq n$ . All the variables  $\mathbf{z} \equiv (z_1, \dots, z_n)$  are coupled to a massive thermostat at temperature  $\tilde{T}$ , and  $\tilde{T} \gg T$ . Then,  $M$  independent simulations using the PBTASS Lagrangian (Equation (10)) are carried out after equilibrating the starting structure with the US bias (Equation (1)). The PBTASS Lagrangian can be setup in a straightforward manner using the recent version of the PLUMED Interface,<sup>50</sup> and a sample input file is given in the Supporting Information.

From the trajectories of these simulations, probability distributions of the CVs,  $\tilde{P}_h(\mathbf{z})$ , for  $h = 1, \dots, M$  simulations, are computed by binning. Subsequently, these biased distributions are reweighted for the bias potential  $V^{\text{pb}}(\bar{\mathbf{z}}, t)$ . Several, but related, reweighting approaches<sup>35,51–55</sup> are available, while for our purpose, we derived a time-dependent reweighting scheme by taking a cue from the work of Tiwary and Parrinello.<sup>53</sup>

If  $\tilde{F}(\mathbf{z})$  is the underlying multidimensional free energy surface at temperature  $\tilde{T}$ , then the biased distribution obtained from a PBTASS simulation corresponding to the

window  $h$  can be written as,

$$\begin{aligned}
 \tilde{P}_h^b(\mathbf{z}, t) &= \frac{\exp\{-\tilde{\beta}\tilde{F}(\mathbf{z})\} \exp\{-\tilde{\beta}V^{\text{pb}}(\bar{\mathbf{z}}, t)\}}{\int d\mathbf{z} \exp\{-\tilde{\beta}[\tilde{F}(\mathbf{z}) + V^{\text{pb}}(\bar{\mathbf{z}}, t)]\}} \\
 &= \frac{\exp\{-\tilde{\beta}\tilde{F}(\mathbf{z})\} \exp\{-\tilde{\beta}V^{\text{pb}}(\bar{\mathbf{z}}, t)\}}{\sum_{j=2}^m \int d\mathbf{z} \exp\{-\tilde{\beta}\tilde{F}(\mathbf{z})\} \exp\{-\tilde{\beta}V_j^b(z_j, t)\}} \\
 &= \frac{\exp\{-\tilde{\beta}\tilde{F}(\mathbf{z})\} \exp\{-\tilde{\beta}V^{\text{pb}}(\bar{\mathbf{z}}, t)\}}{\sum_{j=2}^m \int dz_j \exp\{-\tilde{\beta}\tilde{F}_j(z_j)\} \exp\{-\tilde{\beta}V_j^b(z_j, t)\}} \quad (11)
 \end{aligned}$$

where  $\tilde{\beta} = 1/(k_B \tilde{T})$ , and  $\tilde{F}_j(z_j)$  is the projection of  $\tilde{F}(\mathbf{z})$  along  $z_j$ . The US bias reweighting, which is not considered while deriving the above equation, will be integrated when using the WHAM at the final stage. Here  $j$  runs from 2 to  $m$ , because the first auxiliary variable,  $z_1$  (corresponding to the CV  $s_1$ ), is biased by restraining potential, as shown in Equation (10). It is also emphasized here that  $m \leq n$  because it is not necessary that all the other auxiliary coordinates have to be biased by PBMTD. In the above steps, we used the identity in Equation (5). Unbiased probability distribution  $\tilde{P}_h$  at temperature  $\tilde{T}$  is given by,

$$\tilde{P}_h(\mathbf{z}) = \frac{\exp\{-\tilde{\beta}\tilde{F}(\mathbf{z})\}}{\int d\mathbf{z} \exp\{-\tilde{\beta}\tilde{F}(\mathbf{z})\}} \quad (12)$$

Using Equation (12), we substitute for  $\exp\{-\tilde{\beta}\tilde{F}(\mathbf{z})\}$  in Equation (11) to yield,

$$\begin{aligned}
 \tilde{P}_h^b(\mathbf{z}, t) &= \tilde{P}_h(\mathbf{z}) \frac{\exp\{-\tilde{\beta}V^{\text{pb}}(\bar{\mathbf{z}}, t)\} \int d\mathbf{z} \exp\{-\tilde{\beta}\tilde{F}(\mathbf{z})\}}{\sum_{j=2}^m \int dz_j \exp\{-\tilde{\beta}\tilde{F}_j(z_j)\} \exp\{-\tilde{\beta}V_j^b(z_j, t)\}} \\
 &= \tilde{P}_h(\mathbf{z}) \frac{\exp\{-\tilde{\beta}V^{\text{pb}}(\bar{\mathbf{z}}, t)\}}{\sum_{j=2}^m \left[ \int dz_j \exp\{-\tilde{\beta}\tilde{F}_j(z_j)\} \exp\{-\tilde{\beta}V_j^b(z_j, t)\} / Z_j \right]}
 \end{aligned}$$

where  $Z_j = \int dz_j \exp\{-\tilde{\beta}\tilde{F}_j(z_j)\}$ . On rearranging the above equation, we get the

expression for the unbiased probability distribution as,

$$\begin{aligned}\tilde{P}_h(\mathbf{z}) &= \tilde{P}_h^b(\mathbf{z}, t) \frac{\sum_{j=2}^m \left[ \int dz_j \exp \{ -\tilde{\beta} \tilde{F}_j(z_j) \} \exp \{ -\tilde{\beta} V_j^b(z_j, t) \} / Z_j \right]}{\exp \{ -\tilde{\beta} V^{\text{pb}}(\bar{\mathbf{z}}, t) \}} \\ &= \tilde{P}_h^b(\mathbf{z}, t) \exp \left\{ \tilde{\beta} \left[ V^{\text{pb}}(\bar{\mathbf{z}}, t) + c(t) \right] \right\}\end{aligned}\quad (13)$$

with

$$\begin{aligned}\exp \{ \tilde{\beta} c(t) \} &= \sum_{j=2}^m \left[ \exp \{ -\tilde{\beta} \tilde{F}_j(z_j) \} \exp \{ -\tilde{\beta} V_j^b(z_j, t) \} / Z_j \right] \\ &\approx \sum_{j=2}^m \frac{\int dz_j \exp \{ \tilde{\beta} \gamma V_j^b(z_j, t) \} \exp \{ -\tilde{\beta} V_j^b(z_j, t) \}}{\int dz_j \exp \{ \tilde{\beta} \gamma V_j^b(z_j, t) \}}\end{aligned}$$

where we used Equation (7) and  $\gamma = (\tilde{T} + \Delta T) / \Delta T$ . The last equation becomes exact in the limit  $t \rightarrow \infty$ . Thus, we obtain the relation,

$$c(t) = \tilde{\beta}^{-1} \ln \left[ \sum_{j=2}^m \frac{\int dz_j \exp \{ \tilde{\beta} (\gamma - 1) V_j^b(z_j, t) \}}{\int dz_j \exp \{ \tilde{\beta} \gamma V_j^b(z_j, t) \}} \right] .$$

For each window  $h$ , we can thus obtain the distribution

$$\tilde{P}_h(\mathbf{z}') = \left\langle \prod_i^n \delta(z_i - z'_i) \exp \left\{ \tilde{\beta} \left[ V^{\text{pb}}(\bar{\mathbf{z}}, t) + c(t) \right] \right\} \right\rangle .$$

In practice, the above can be implemented by a time-dependent binning of the time series data of the auxiliary variables as,

$$\tilde{P}_h(\mathbf{z}') = \frac{\int_{t_{\min}}^{t_{\max}} d\tau \exp \{ \tilde{\beta} [V^{\text{pb}}(\bar{\mathbf{z}}, t) + c(t)] \} \prod_{i=1}^n \delta(\mathbf{z}_i - \mathbf{z}'_i)}{\int_{t_{\min}}^{t_{\max}} d\tau \exp \{ \tilde{\beta} [V^{\text{pb}}(\bar{\mathbf{z}}, t) + c(t)] \}} . \quad (14)$$

In our calculations,  $t_{\min}$  was set as the first time-step of PBTASS and  $t_{\max}$  was varied

till a satisfactory convergence in free energy estimates was observed. Although varying  $t_{\min}$  didn't make any difference in our calculations, it may become important to choose a suitable value when PBTASS simulation is not started from a good initial structure and when the initial bias growth rate is very high.

Subsequently,  $M$  distributions  $\{\tilde{P}_h\}$ , as obtained using Equation (14), are combined to get  $\tilde{P}(\mathbf{z})$  using WHAM, exercising Equation (2), and the free energy surface  $F(\mathbf{z})$  for temperature  $T$  is computed using Equation (8). For bias reweighting and performing WHAM, we have developed our own programs.

It is better to perform WHAM on low dimensional distributions. For this purpose, the probability distribution of each slice may be projected to a set of relevant low dimensions before carrying out WHAM. A more general mean-force-based approach<sup>56–58</sup> can be formulated to combine the free energy slices in this case, thereby evading WHAM. This will be communicated in a forthcoming publication.

### 3 Results and Discussion

#### 3.1 Alanine Tripeptide *In Vacuo*

At first, we investigated the free energetics of alanine tripeptide *in vacuo* to benchmark the PBTASS method. MD calculations were performed using AMBER14<sup>59</sup> interfaced with PLUMED-2.2.3.<sup>60</sup> The ff14SB force field<sup>59</sup> was taken to describe interatomic interactions. We chose four Ramachandran angles  $(\phi_1, \psi_1, \phi_2, \psi_2)$  as CVs and the free energy surface  $F(\phi_1, \psi_1, \phi_2, \psi_2)$  was computed using PBTASS, TASS, TAMd, and PBMTD methods; see Figure 1 for the definition of CVs.

In PBTASS simulations, we chose  $\phi_1$  for applying the umbrella bias. A three-dimensional PBMTD bias,  $V^{\text{pb}}(\psi_1, \phi_2, \psi_2)$ , was applied along the CVs  $\psi_1$ ,  $\phi_2$ , and  $\psi_2$ . As in Equation (5), the three-dimensional bias was constructed based on the three one-

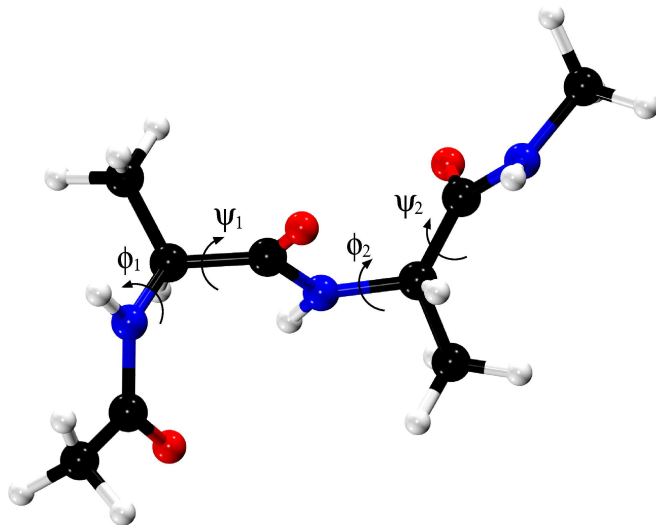


Figure 1: Alanine tripeptide molecule is shown where the four Ramachandran angles ( $\phi_1, \psi_1, \phi_2, \psi_2$ ) chosen as CVs are labelled. Atom color codes: Black (C); Blue (N); Red (O); White (H).

dimensional MTD biases  $V^b(\psi_1)$ ,  $V^b(\phi_2)$ , and  $V^b(\psi_2)$ . The choice of the type of the bias applied along a CV was arbitrary for this problem. An overdamped Langevin thermostat with a friction coefficient of  $0.1 \text{ fs}^{-1}$  was used to maintain the auxiliary variable temperature at 3000 K. The PBMTD bias potential was updated every 500 fs, and the bias parameters  $w_1(0) = w_2(0) = w_3(0) = 0.6 \text{ kcal mol}^{-1}$  and  $\delta s = 0.05$  radians were taken. The parameter  $\Delta T$  was set to 21000 K in order to achieve a reasonable bias growth rate. The umbrella potential was applied from  $-\pi$  to  $\pi$  at an interval of 0.2 radians with  $\kappa_h = 1.2 \times 10^2 \text{ kcal mol}^{-1} \text{ rad}^{-2}$ ,  $k_i = 1.2 \times 10^3 \text{ kcal mol}^{-1} \text{ rad}^{-2}$ , and  $\mu_i = 50 \text{ amu } \text{\AA}^2 \text{ rad}^{-2}$ , for  $h = 1, \dots, 33$  and  $i = 1, \dots, 4$ . Langevin thermostat with a friction coefficient of  $0.1 \text{ fs}^{-1}$  was used for maintaining the temperature of physical system at 300 K. Before starting the PBTASS simulation for a specific window, we carried out equilibration for 100 ps. Starting structures for the equilibration runs were taken as the global minimum structure of alanine tripeptide for all the windows.

For TASS, TAMd, and PBMTD runs, we used identical set up as that of the PBTASS simulation. In TASS, the MTD bias (Equation (3)) was applied only along  $\phi_2$ . For the

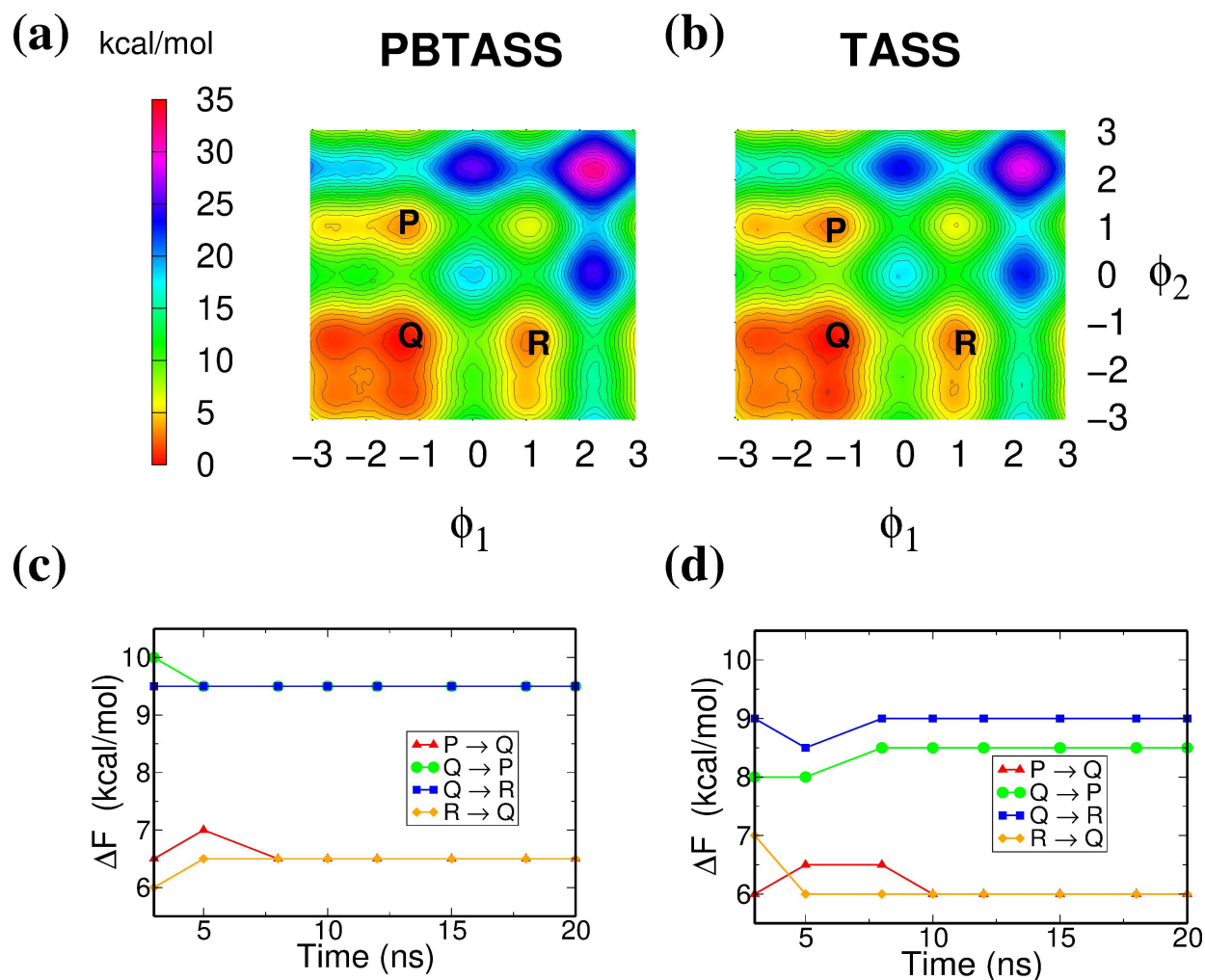


Figure 2: The free energy surface  $F(\phi_1, \phi_2)$  of alanine tripeptide *in vacuo* computed from (a) PBTASS and (b) TASS simulations after 20 ns per window. Contours are drawn for every 1 kcal mol<sup>-1</sup>. Convergence of various free energy barriers on these surfaces as a function of simulation time per window is shown in the lower panels (c) and (d).

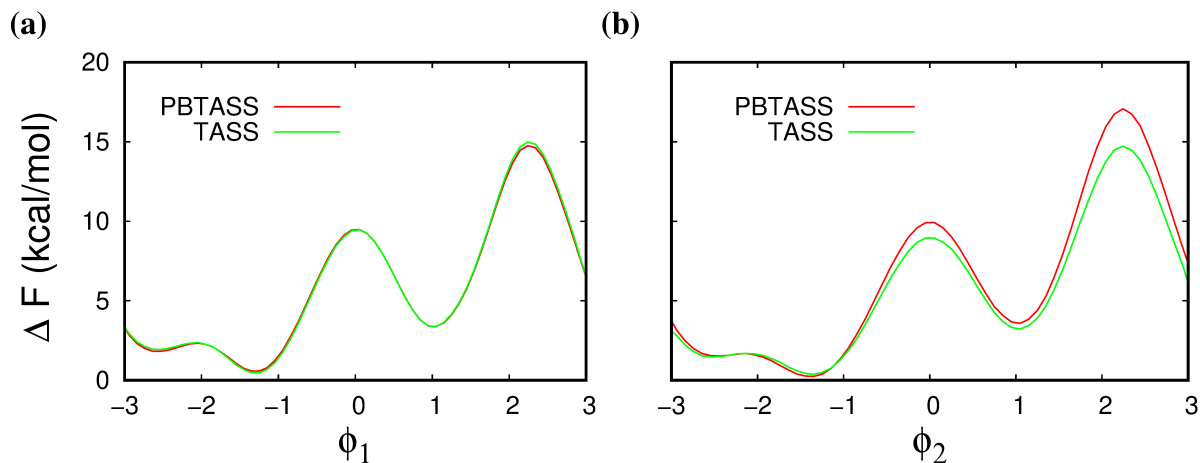


Figure 3: (a)  $F(\phi_1)$ , and (b)  $F(\phi_2)$  for alanine tripeptide *in vacuo* computed from PBTASS (red) and TASS (green) simulations after 20 ns per window. Here angles are in radians.

benefit of comparison, the parameters used in these simulations were kept the same as that used in PBTASS runs. In PBMTD reference simulations, bias potential was applied only along  $\phi_1$  and  $\phi_2$ .

Four-dimensional free energy surface  $F(\phi_1, \psi_1, \phi_2, \psi_2)$  was computed from the PBTASS trajectory using the method described in Section 2, and the high dimensional surface was projected on the  $(\phi_1, \phi_2)$  space for analysis; See Figure 2. The three main metastable states on the  $F(\phi_1, \phi_2)$  free energy surface are labelled as **P**, **Q**, and **R**. The converged free energy barriers **Q**→**R** and **Q**→**P** are  $9.5 \text{ kcal mol}^{-1}$ , while the reverse barriers, i.e. **P**→**Q** and **R**→**Q**, are  $6.5 \text{ kcal mol}^{-1}$ . Of great importance, the free energy barriers are converged within  $\sim 8 \text{ ns}$  (per window). It is also gratifying to see that the diagonal reflection symmetry<sup>44</sup> of the  $F(\phi_1, \phi_2)$  surface is retained.

On the other hand, the free energy barriers computed using TASS are converged to values within  $\sim 1 \text{ kcal mol}^{-1}$  of that computed from PBTASS; See also Table 1. Ideally, the **Q**→**R** and **Q**→**P** barriers have to be the same (due to the symmetry of the surface), however, a small difference ( $\sim 0.5 \text{ kcal mol}^{-1}$ ) is noticed. This could be due to poor

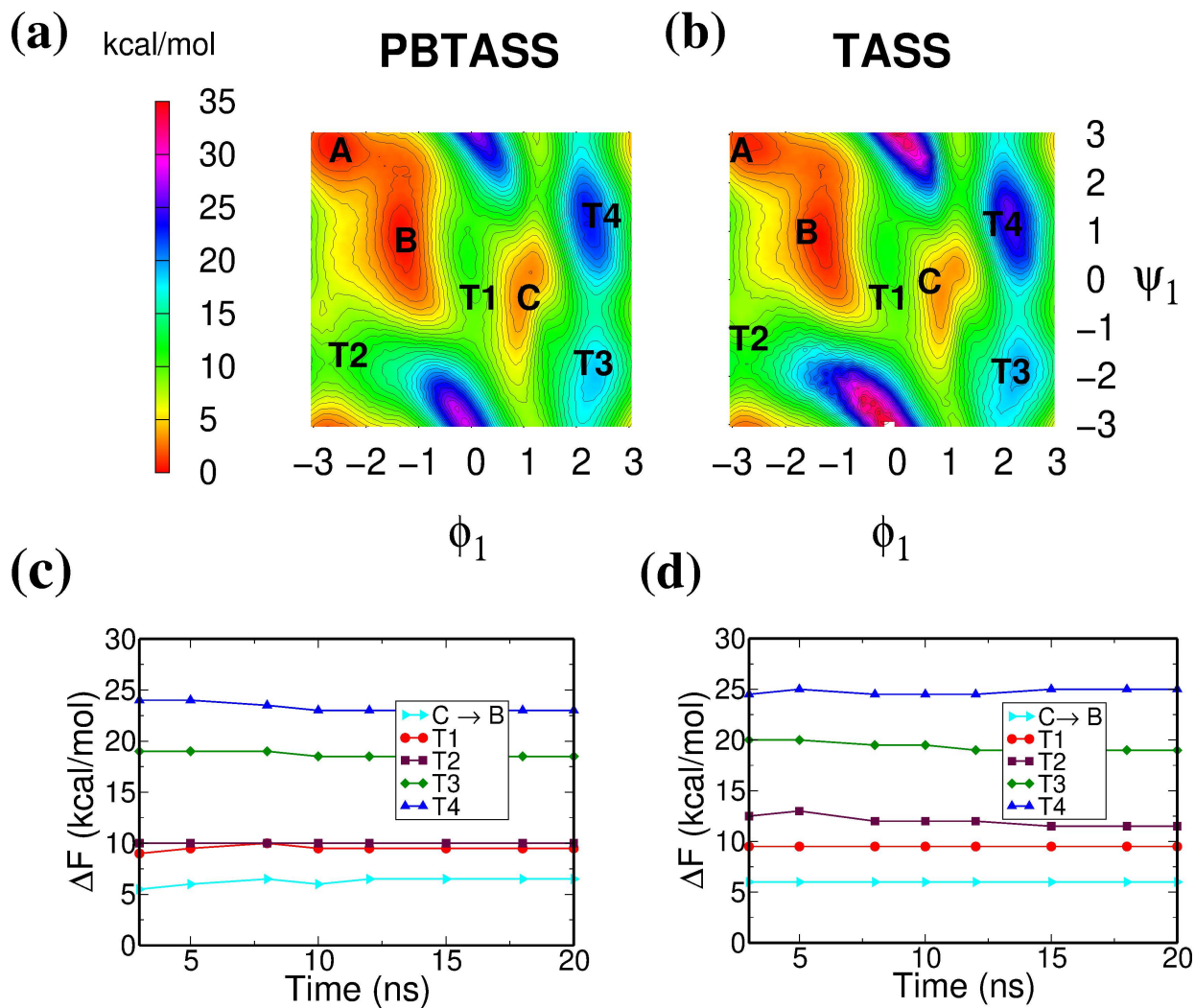


Figure 4: The free energy surface  $F(\phi_1, \psi_1)$  of alanine tripeptide *in vacuo* computed from (a) PBTASS and (b) TASS simulations after 20 ns per window. Contours are drawn for every 1 kcal mol<sup>-1</sup>. Convergence of free energy barrier for  $B \rightarrow C$ , and free energies of the saddle points T1, T2, T3, and T4 with respect to the free energy of B as a function of simulation time per window in PBTASS (c), and TASS (d) runs are also shown in the lower panels. Here angles are in radians.



convergence of free energy along  $\phi_2$ , where the MTD bias potential with a high value of  $\Delta T$  was applied in TASS. After 10 ns, reverse barriers were found to be the same and equal to 6 kcal mol<sup>-1</sup>.

The one-dimensional projections of  $F(\phi_1, \psi_1, \phi_2, \psi_2)$  along  $\phi_1$  and  $\phi_2$  were computed for the TASS and PBTASS cases, and are given in Figure 3.  $F(\phi_1)$  computed using TASS and PBTASS methods agrees well with each other, while  $F(\phi_2)$  shows a difference of up to 3 kcal mol<sup>-1</sup>. This indicates that some parts of the high dimensional free energy landscape are not converged in TASS, as a result of the high  $\Delta T$ .

For further analysis, we projected the four-dimensional free energy surfaces to  $(\phi_1, \psi_1)$ , and  $(\phi_2, \psi_2)$  spaces; See Figure 4 and Figure S1. Our main interest was not only to compare the convergence of barriers, but also to check the convergence of free energies of saddle points where the sampling is apparently poor. We notice that the free energy barrier for **C**→**B** converges quickly and the results from PBTASS and TASS simulations are in good agreement. The free energies of both **T1** and **T2** saddle points are nearly identical in PBTASS, while they deviate about 2 kcal mol<sup>-1</sup> in TASS (Table 1). The free energy of **T3** is also nearly the same in both methods. The highest energy saddle point **T4** was found to converge quickly in PBTASS compared to TASS. Similar observation can be also made while analyzing the free energy landscape  $F(\phi_2, \psi_2)$ ; See Figure S1. These results are assuring the accuracy and efficiency of PBTASS in exploring high dimensional free energy landscapes.

Finally, we compare the performance of PBTASS with TAMD and PBMTD methods. The free energy surface  $F(\phi_1, \phi_2)$  obtained from the TAMD and PBMTD calculations are shown in Figure 5. It can be clearly seen that, even after 20 ns, the exploration of the free energy surface is not as exhaustive as that observed in PBTASS and TASS simulations. The TAMD and PBMTD free energy surfaces are more noisy and the free energy barriers **Q** → **P** and **Q** → **R** are 10.0 and 9.0 kcal mol<sup>-1</sup>, respectively, with

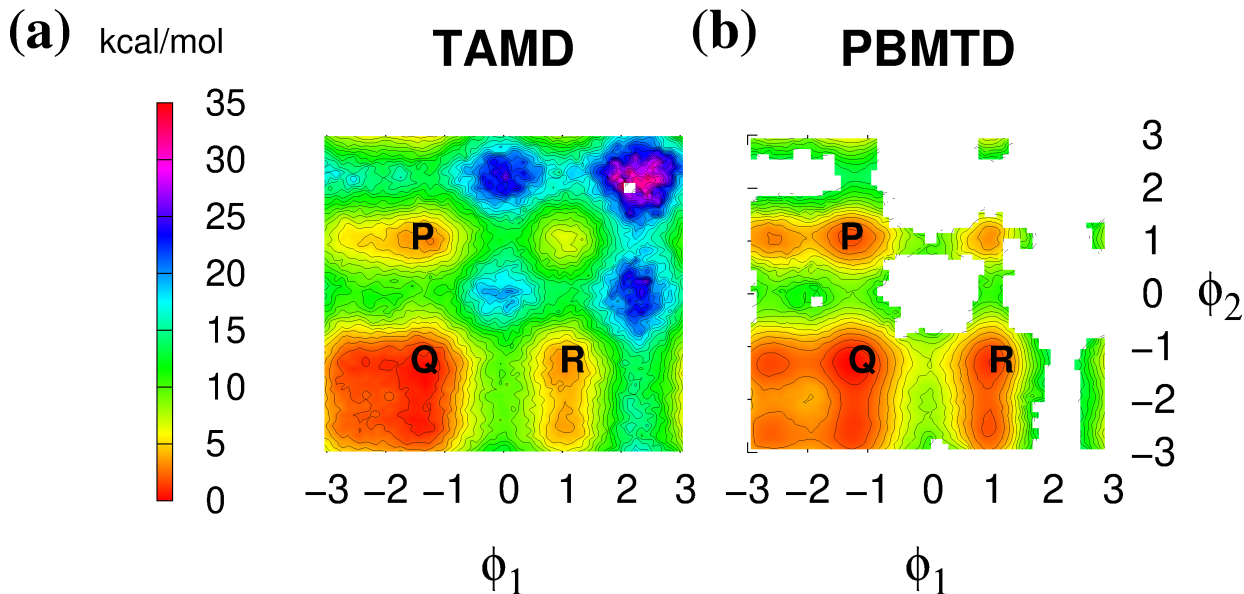


Figure 5: The free energy surface  $F(\phi_1, \phi_2)$  of alanine tripeptide *in vacuo* computed from (a) TAMD and (b) PBMTD simulations after 20 ns are presented. Here angles are in radians. Contours are drawn for every 1 kcal mol<sup>-1</sup>.

TAMD, while they are 9.8 and 7.3 kcal mol<sup>-1</sup>, respectively, with PBMTD (Table 1). Although the exploration of high energy regions is much better with TAMd than PBMTD, detailed analysis show that the high energy regions of the landscape are not properly converged within 20 ns, unlike we observed in PBTASS runs. This is apparent in Figure S2. Clearly, in PBTASS runs, the system was able to diffuse through the entire four-dimensional CV-space in a more exhaustive manner compared to other methods. This capability of PBTASS can be ascribed to the inherent divide-and-conquer procedure invoked by the US bias, in addition to the boosted sampling rendered through the combination of high temperature and parallel bias.

Clearly, these results show that PBTASS is as accurate and efficient as TASS, while outperforms TAMd, and PBMTD methods.

Table 1: Free energies barriers ( $\Delta F^\ddagger$ ) and free energies ( $\Delta F$ ) of the saddle points (compared to the free energy of **A**) computed after 20 ns using PBTASS, TASS, TAMD, and PBMTD simulations. Free energies are in kcal mol<sup>-1</sup>. Dash symbol (–) indicates that the corresponding free energies could not be computed due to noise arising from poor sampling.

Method	$\Delta F^\ddagger$				$\Delta F$			
	<b>Q</b> $\rightarrow$ <b>P</b>	<b>Q</b> $\rightarrow$ <b>R</b>	<b>P</b> $\rightarrow$ <b>Q</b>	<b>R</b> $\rightarrow$ <b>Q</b>	<b>T1</b>	<b>T2</b>	<b>T3</b>	<b>T4</b>
PBTASS	9.5	9.5	6.5	6.5	9.4	10.0	18.8	23.1
TASS	8.5	9.0	6.0	6.0	9.3	11.6	19.3	25.3
TAMD	10.0	9.0	7.0	5.5	9.0	7.0	18.0	–
PBMTD	9.8	7.3	7.3	6.0	6.2	–	–	–

### 3.2 Alanine Pentapeptide *In Vacuo*

As an application of PBTASS, we carried out a detailed study of alanine pentapeptide *in vacuo* aimed to compute the eight-dimensional free energy surface as a function of eight Ramachandran angles ( $\phi_1, \psi_1, \phi_2, \psi_2, \phi_3, \psi_3, \phi_4, \psi_4$ ); see Figure 6. MD calculations were performed using AMBER14<sup>59</sup> interfaced with PLUMED-2.2.3.<sup>60</sup> We chose the ff14SB force field<sup>59</sup> for these simulations.

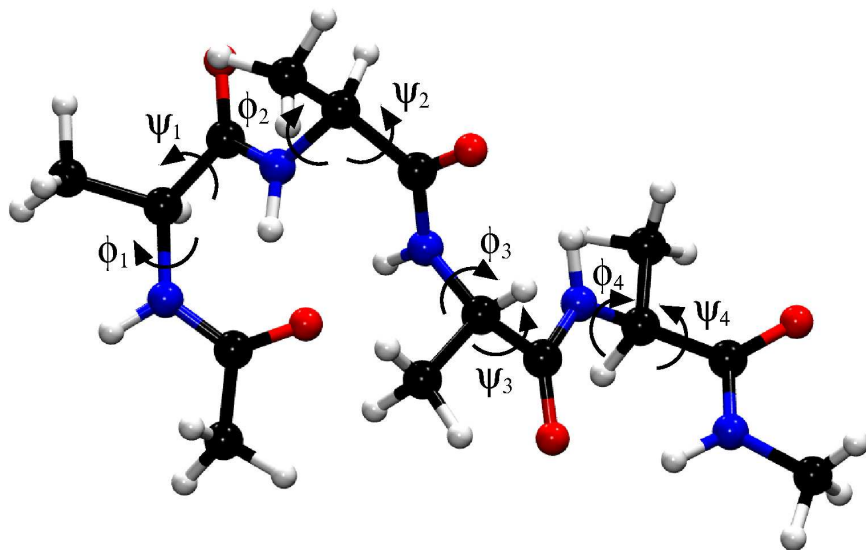


Figure 6: Alanine pentapeptide molecule is shown, where the eight Ramachandran angles that are taken as CVs are labeled.

All the eight Ramachandran angles were taken as CVs in our PBTASS simulations. Here we have arbitrarily opted the  $\phi_2$  coordinate for applying the US bias. The parallel (three-dimensional) MTD biases were applied along the other three  $\phi$  angles, i.e.  $(\phi_1, \phi_3, \phi_4)$ . All the eight auxiliary variables were thermostatted at 3000 K. An overdamped Langevin thermostat with a friction coefficient of  $0.1 \text{ fs}^{-1}$  was used to maintain their temperature. The PBMTD bias potential was updated every 500 fs and the PBMTD parameters  $w_1(0) = w_2(0) = w_3(0) = 0.6 \text{ kcal mol}^{-1}$  and  $\delta s = 0.05$  radians were taken. The parameter  $\Delta T$  was set to 45000 K. The umbrella potential was applied from  $-\pi$  to  $\pi$  at an interval of 0.2 radians with  $\kappa_h = 1.2 \times 10^2 \text{ kcal mol}^{-1} \text{ rad}^{-2}$ ,  $k_i = 1.2 \times 10^3 \text{ kcal mol}^{-1} \text{ rad}^{-2}$ , and  $\mu_i = 50 \text{ amu } \text{\AA}^2 \text{ rad}^{-2}$ , for  $h = 1, \dots, 33$  and  $i = 1, \dots, 8$ . We used the same setups for doing TASS, TAMd, and PBMTD simulations. In TASS, we applied the US bias along  $\phi_2$  and one-dimensional MTD bias along  $\phi_1$ . In PBMTD simulations, we chose the four  $\phi$  angles as CVs.

The high dimensional free energy surface obtained after 25 ns (per window) of PBTASS simulation was projected to  $(\phi_1, \phi_2)$  space and the convergence of the free energy barriers were analyzed; See Figure 7. Considering the dimensionality of the explored surface, the extent of sampling and the observed smoothness of the projected surfaces are remarkable. All the regions in the  $(\phi_1, \phi_2)$  space, including all the 2<sup>nd</sup> order saddles were sampled well. Free energy barriers separating various metastable states and the free energy of saddle points on this surface were computed and their convergence was analyzed. The computed free energy barriers for  $\mathbf{M} \rightarrow \mathbf{L}$  and  $\mathbf{M} \rightarrow \mathbf{N}$  are nearly the same and they converged quickly in PBTASS. The same was also seen for the reverse reactions; see also Table 2. A quick convergence of the free energies of the high energy saddle points was also observed in the PBTASS simulation (Figure 7).

The same analysis was also extended for TASS simulation. Interestingly, free energy barriers computed from TASS runs are close to that computed from PBTASS simulations

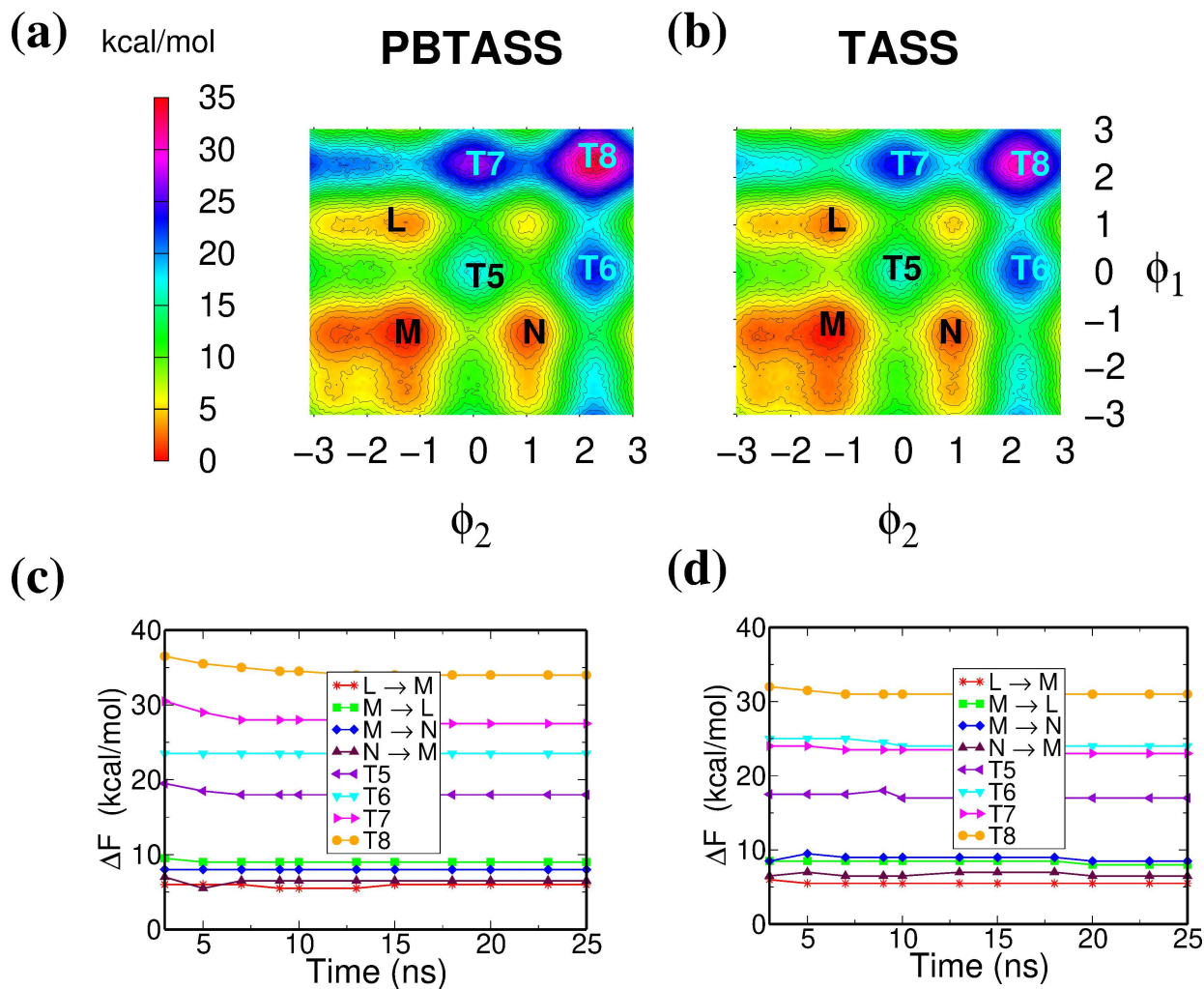


Figure 7: The free energy surface  $F(\phi_1, \phi_2)$  of alanine pentapeptide *in vacuo* computed from (a) PBTASS and (b) TASS simulations after 25 ns per window. Some of the conformational states are labelled as L, M, N, T5, T6, T7 and T8. Contours are drawn for every 1 kcal mol<sup>-1</sup>. Convergence plots of some of the free energy barriers and free energies of saddle points with respect to the minimum M as a function of time per window are shown in the lower panels (c) and (d).

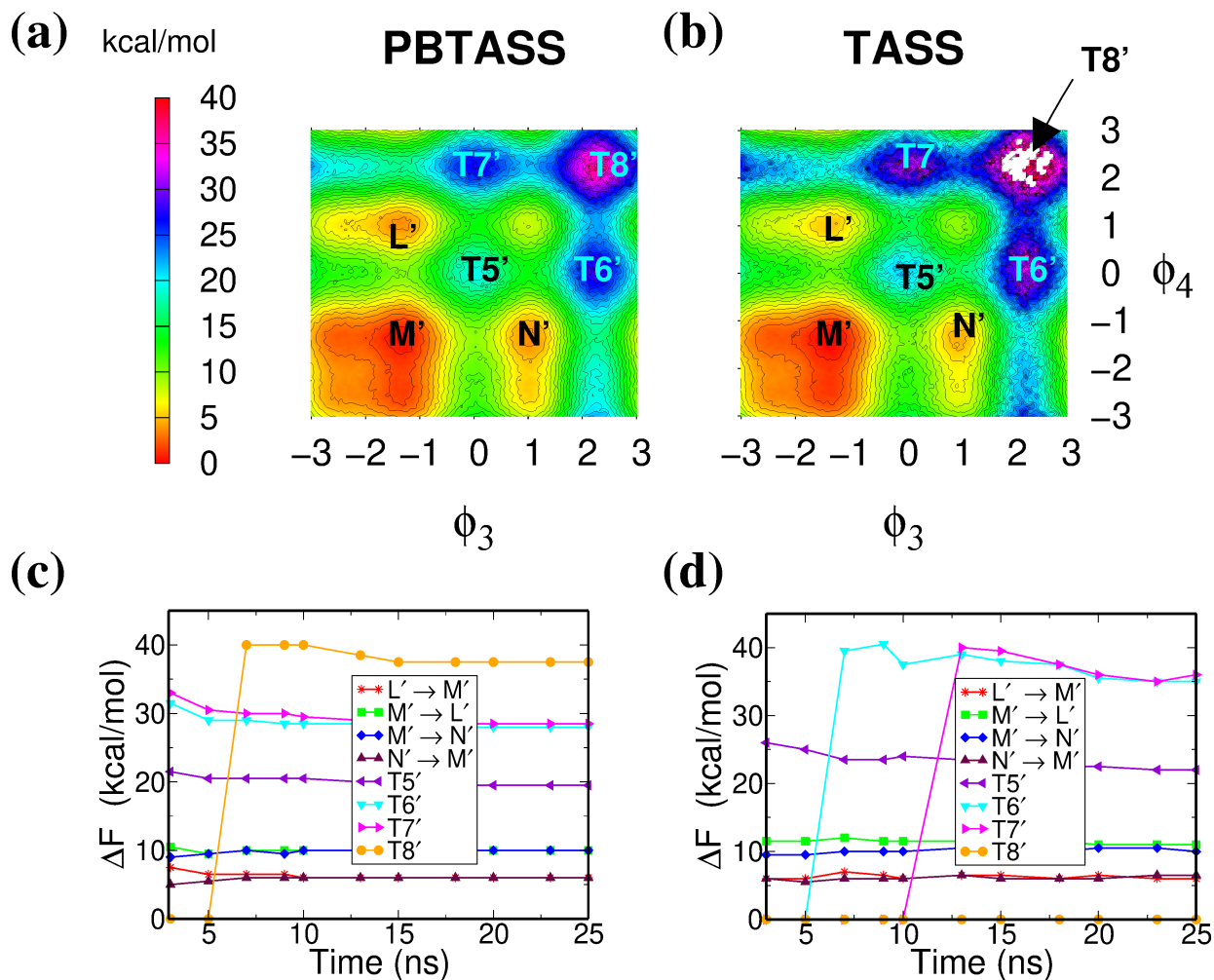


Figure 8: The free energy surface  $F(\phi_3, \phi_4)$  of alanine pentapeptide *in vacuo* computed from (a) PBTASS and (b) TASS simulations after 25 ns per window. Some of the conformational states are labelled as  $L'$ ,  $M'$ ,  $N'$ ,  $T5'$ ,  $T6'$ ,  $T7'$  and  $T8'$ . Contours are drawn for every 1 kcal mol<sup>-1</sup>. Convergence plots of some of the free energy barriers and free energies of saddle points with respect to the minimum  $M'$  as a function of time per window are shown in the lower panels (c) and (d). Undetermined free energies (due to poor sampling) are indicated as zero.



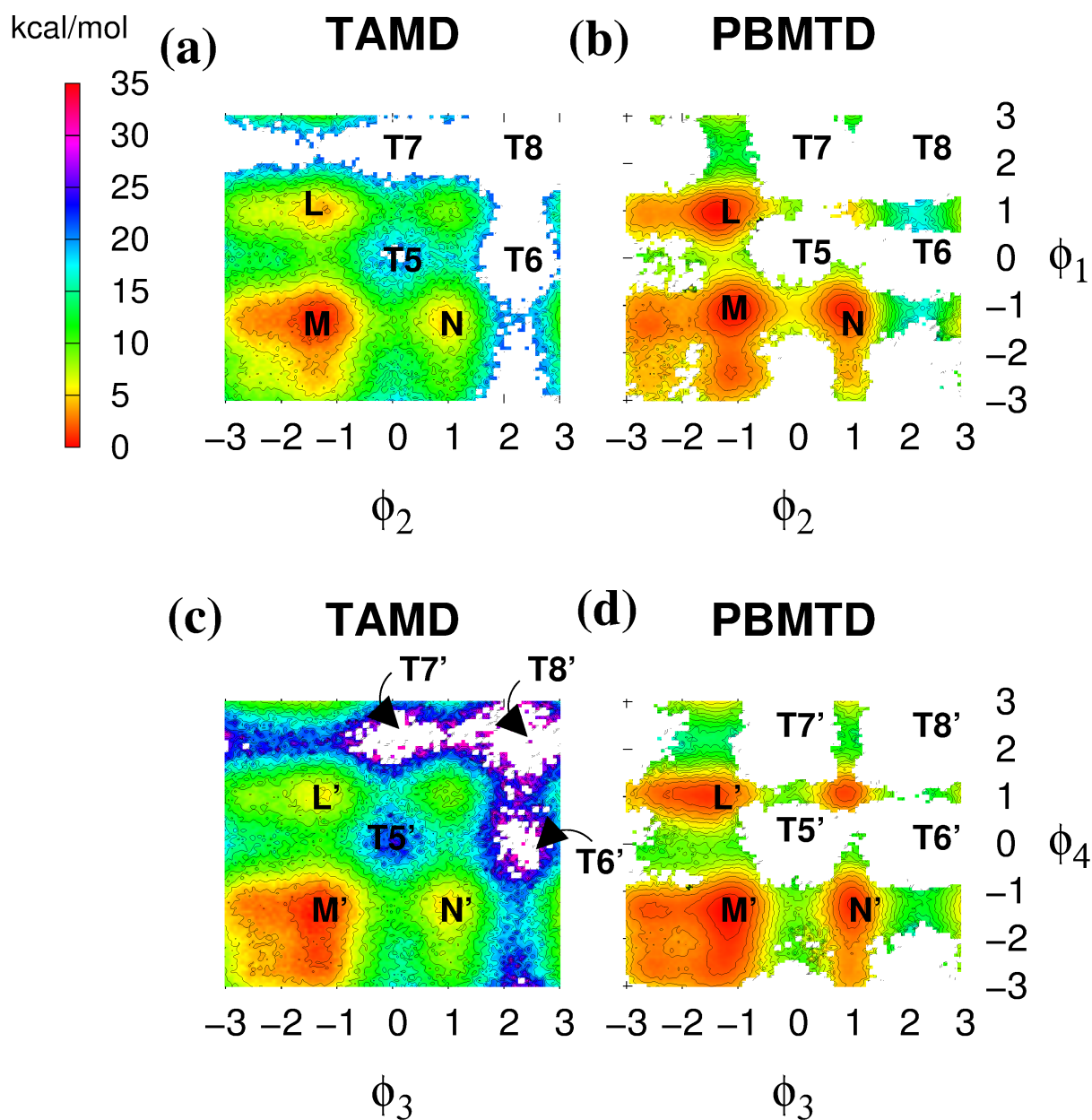


Figure 9: The free energy surfaces  $F(\phi_1, \phi_2)$  (top panel) and  $F(\phi_3, \phi_4)$  (bottom panel) of alanine pentapeptide *in vacuo* computed from TAMD (left panel) and PBMTD (right panel) simulations after 25 ns. Here angles are in radians. Contours are drawn for every 1 kcal mol<sup>-1</sup>. White patches on the surfaces show that the sampling of these regions was not adequate enough for estimating free energies.

(Table 2, Figure 7). However, the free energies of some of the saddle points show large deviations from the PBTASS results.

As next, the free energy surfaces  $F(\phi_3, \phi_4)$  computed using PBTASS and TASS methods are compared (Figure 8). The convergence of free energy barriers are quick in both these methods, and they agree well with each other. However, most striking difference between PBTASS and TASS can be seen in the convergence of the free energies of the saddle points. Especially, the **T8'** saddle point was not sampled well enough to resolve in TASS, but the sampling was acceptable in PBTASS. This lead us to conclude that the differences in the estimates of free energies of saddle points from PBTASS and TASS simulations are resulting from the poor exploration of saddle point regions in TASS compared to PBTASS. Analyses of other projections of the free energy surface also yield the same conclusions (See Figure S3, S4, and Table S1).

Free energy surfaces  $F(\phi_1, \phi_2)$  and  $F(\phi_3, \phi_4)$  computed using TAMD, and PBMTD methods are shown in Figure 9. Both TAMD and PBMTD simulations were of 25 ns long. It can be seen that low free energy regions of the CV-space were sampled reasonably well by both the methods. However, some of the free energy barriers computed from TAMD and PBMTD deviated up to 2 kcal mol<sup>-1</sup> from the PBTASS estimates; See Table 2. Free energies of several saddle points on the surfaces were not computable from the TAMD and PBMTD simulations as a consequence of poor sampling.

These results show that the PBTASS approach outperforms the other three methods. The PBTASS method is able to thoroughly sample the eight-dimensional surface of alanine pentapeptide and could provide reliable free energy estimates within an affordable simulation time.



Table 2: Free energies barriers and free energies of the saddle points (compared to the free energy of **M** or **M'**) from free energy surfaces for alanine pentapeptide *in vacuo* as in Figures 7 and 8 computed using PBTASS, TASS, TAMD, and PBMTD methods after 25 ns. Free energies are in kcal mol<sup>-1</sup>.

Method	$\Delta F^\ddagger$				$\Delta F$			
	<b>M</b> $\rightarrow$ <b>L</b>	<b>M</b> $\rightarrow$ <b>N</b>	<b>L</b> $\rightarrow$ <b>M</b>	<b>N</b> $\rightarrow$ <b>M</b>	<b>T5</b>	<b>T6</b>	<b>T7</b>	<b>T8</b>
PBTASS	8.9	8.0	5.9	6.6	17.8	23.5	27.5	34.0
TASS	8.0	8.5	5.5	6.9	16.7	22.9	24.1	31.1
TAMD	9.4	10.3	5.9	5.9	23.6	-	-	-
PBMTD	5.2	6.6	4.6	6.5	-	-	-	-
	<b>M'</b> $\rightarrow$ <b>L'</b>	<b>M'</b> $\rightarrow$ <b>N'</b>	<b>L'</b> $\rightarrow$ <b>M'</b>	<b>N'</b> $\rightarrow$ <b>M'</b>	<b>T5'</b>	<b>T6'</b>	<b>T7'</b>	<b>T8'</b>
PBTASS	10.0	9.8	6.3	6.2	19.6	28.5	27.6	37.5
TASS	10.9	10.1	5.9	5.6	22.1	35.3	35.2	-
TAMD	11.5	11.0	6.1	5.6	25.0	-	-	-
PBMTD	9.1	8.2	8.0	7.3	-	-	-	-

## 4 Conclusions

The PBTASS method introduced in this work combines the PBMTD high dimensional bias with the TASS Lagrangian. This brings a major boost in the efficiency of TASS in sampling a high dimensional CV-space. We have demonstrated the accuracy and the efficiency of this method in exploring high dimensional free energy surfaces, and for free energy calculations by taking the examples of alanine tripeptide and alanine pentapeptide.

The advantage of the PBTASS method over TASS is that it can bias more number of CVs and can enhance the sweeping motion of the system in a high dimensional CV-space while retaining all the salient features of the original TASS method.<sup>44</sup> Thus, the PBTASS method is a promising alternative to TASS, TAMD, PBMTD, and similar methods, for calculating free energies of chemical reactions and structural transformations occurring in large soft matter systems. Substantial progress has been made in using machine learning tools to determine order parameters in describing rare-events.<sup>61–66</sup> Methods like PBTASS, which enables the system to transverse through a high dimen-

sional CV-space in an exhaustive manner, are most suited to be integrated with machine learning tools.<sup>67</sup> This will be our focus in the near future.

## Acknowledgments

Authors acknowledge the HPC facility (HPC2013) at the Indian Institute of Technology Kanpur. AG and SV thank the DST-INSPIRE for their Ph.D. fellowship.

## References

- (1) Peters, B. *Reaction Rate Theory and Rare Events*; Elsevier: Amsterdam, Netherlands, 2017.
- (2) Tuckerman, M. E. *Statistical Mechanics: Theory and Molecular Simulation*, 1st ed.; Oxford University Press: Oxford, 2010.
- (3) Vanden-Eijnden, E. Some Recent Techniques for Free Energy Calculations. *J. Comput. Chem.* **2009**, *30*, 1737.
- (4) Christ, C. D.; Mark, A. E.; van Gunsteren, W. F. Basic ingredients of free energy calculations: A review. *J. Comput. Chem.* **2010**, *31*, 1569–1582.
- (5) Bonella, S.; Meloni, S.; Ciccotti, G. Theory and Methods for Rare Events. *Eur. Phys. J. B* **2012**, *85*, 97.
- (6) Valsson, O.; Tiwary, P.; Parrinello, M. Enhancing Important Fluctuations: Rare Events and Metadynamics from a Conceptual Viewpoint. *Annu. Rev. Phys. Chem.* **2016**, *67*, 159.

- (7) Awasthi, S.; Nair, N. N. Exploring high-dimensional free energy landscapes of chemical reactions. *Wiley Interdiscip. Rev. Comput. Mol. Sci.* **9**, e1398.
- (8) Paul, S.; Nair, N. N.; Harish, V. Phase space and collective variable based simulation methods for studies of rare events. *Mol. Sim.* **2019**, *45*, 1273–1284.
- (9) Torrie, G. M.; Valleau, J. P. Monte Carlo Free Energy Estimates Using Non-Boltzmann Sampling: Application to the Sub-critical Lennard-Jones Fluid. *Chem. Phys. Lett.* **1974**, *28*, 578.
- (10) Kästner, J. Umbrella Sampling. *Wiley Interdiscip. Rev.* **2011**, *1*, 932.
- (11) Ferrenberg, A. M.; Swendsen, R. H. Optimized Monte Carlo Data Analysis. *Phys. Rev. Lett.* **1989**, *63*, 1195.
- (12) Kumar, S.; Rosenberg, J. M.; Bouzida, D.; Swendsen, R. H.; Kollman, P. A. The Weighted Histogram Analysis Method for Free-energy Calculations on Biomolecules. I. The Method. *J. Comput. Chem.* **1992**, *13*, 1011.
- (13) Laio, A.; Parrinello, M. Escaping Free-energy Minima. *Proc. Natl. Acad. Sci. U.S.A* **2002**, *99*, 12562.
- (14) Iannuzzi, M.; Laio, A.; Parrinello, M. Efficient Exploration of Reactive Potential Energy Surfaces Using Car-Parrinello Molecular Dynamics. *Phys. Rev. Lett.* **2003**, *90*, 238302.
- (15) Barducci, A.; Bussi, G.; Parrinello, M. Well-Tempered Metadynamics: A Smoothly Converging and Tunable Free-Energy Method. *Phys. Rev. Lett.* **2008**, *100*, 020603.
- (16) Laio, A.; Parrinello, M. In *Computer simulations in condensed matter: From materials to chemical biology*; Ferrario, M., Ciccotti, G., Binder, K., Eds.; Springer: Berlin, 2006; Vol. 1.

- (17) Ensing, B.; Vivo, M. D.; Liu, Z.; Moore, P.; Klein, M. L. Metadynamics as a Tool for Exploring Free Energy Landscapes of Chemical Reactions. *Acc. Chem. Res.* **2006**, *39*, 73.
- (18) Laio, A.; Gervasio, F. L. Metadynamics: a method to simulate rare events and reconstruct the free energy in biophysics, chemistry and material science. *Rep. Prog. Phys* **2008**, *71*, 126601.
- (19) Barducci, A.; Bonomi, M.; Parrinello, M. Metadynamics. *Wiley Interdiscip. Rev. Comput. Mol. Sci.* **2011**, *1*, 826.
- (20) Sutto, L.; Marsili, S.; Gervasio, F. L. New advances in metadynamics. *Wiley Interdiscip. Rev. Comput. Mol. Sci.* **2012**, *2*, 771–779.
- (21) Abrams, C.; Bussi, G. Enhanced Sampling in Molecular Dynamics Using Metadynamics, Replica-Exchange, and Temperature-Acceleration. *Entropy* **2014**, *16*, 163.
- (22) Bussi, G.; Branduardi, D. *Reviews in Computational Chemistry Volume 28*; Wiley-Blackwell, 2015; Chapter 1, pp 1–49.
- (23) Pietrucci, F. Strategies for the exploration of free energy landscapes: Unity in diversity and challenges ahead. *Rev. Phys.* **2017**, *2*, 32–45.
- (24) Allison, J. Computational methods for exploring protein conformations. *Biochem. Soc. Trans.* **2020**, *48*, 1707–1724.
- (25) Bussi, G.; Laio, A.; Tiwary, P. In *Handbook of Materials Modeling: Methods: Theory and Modeling*; Andreoni, W., Yip, S., Eds.; Springer International Publishing: Cham, 2020; pp 565–595.
- (26) Piana, S.; Laio, A. A Bias-Exchange Approach to Protein Folding. *J. Phys. Chem. B* **2007**, *111*, 4553.

- (27) Marinelli, F.; Pietrucci, F.; Laio, A.; Piana, S. A Kinetic Model of Trp-Cage Folding from Multiple Biased Molecular Dynamics Simulations. *PLoS Comput. Biol.* **2009**, *5*, e1000452.
- (28) Pfaendtner, J.; Bonomi, M. Efficient Sampling of High-Dimensional Free-Energy Landscapes with Parallel Bias Metadynamics. *J. Chem. Theory Comput.* **2015**, *11*, 5062.
- (29) Prakash, A.; Fu, C. D.; Bonomi, M.; Pfaendtner, J. Biasing Smarter, Not Harder, by Partitioning Collective Variables into Families in Parallel Bias Metadynamics. *J. Chem. Theory Comput.* **2018**, *14*, 4985–4990.
- (30) Zhao, M.; Sampat, J.; Alamdari, S.; Shen, G.; Chen, C.-L.; Mundy, C.; Pfaendtner, J.; Ferguson, A. MARTINI-Compatible Coarse-Grained Model for the Mesoscale Simulation of Peptoids. *J. Phys. Chem. B* **2020**, *124*, 7745–7764.
- (31) Buckle, E.; Prakash, A.; Bonomi, M.; Sampath, J.; Pfaendtner, J.; Drobny, G. Solid-State NMR and MD Study of the Structure of the Statherin Mutant SNa15 on Mineral Surfaces. *J. Am. Chem. Soc.* **2019**, *141*, 1998–2011.
- (32) Sala, B.; Marchand, T.; Pintacuda, G.; Camilloni, C.; Natalello, A.; Ricagno, S. Conformational Stability and Dynamics in Crystals Recapitulate Protein Behavior in Solution. *Biophys. J.* **2020**, *119*, 978–988.
- (33) Arsiccio, A.; McCarty, J.; Pisano, R.; Shea, J. Heightened Cold-Denaturation of Proteins at the Ice–Water Interface. *J. Am. Chem. Soc.* **2020**, *142*, 5722–5730.
- (34) Schmid, R.; Nielaba, P. Stability of nanoparticles in solution: A statistical description of crystallization as a finite particle size effect in a lattice-gas model. *J. Chem. Phys.* **2019**, *150*, 054504.

- (35) Invernizzi, M.; Parrinello, M. Rethinking Metadynamics: From Bias Potentials to Probability Distributions. *J. Phys. Chem. Lett.* **2020**, *11*, 2731–2736.
- (36) Invernizzi, M.; Parrinello, M. Making the Best of a Bad Situation: A Multiscale Approach to Free Energy Calculation. *J. Chem. Theory Comput.* **2019**, *15*, 2187–2194.
- (37) Oshima, H.; Re, S.; Sugita, Y. Replica-Exchange Umbrella Sampling Combined with Gaussian Accelerated Molecular Dynamics for Free-Energy Calculation of Biomolecules. *J. Chem. Theory Comput.* **2019**, *16*, 5199–5208.
- (38) Valsson, O.; Parrinello, M. In *Handbook of Materials Modeling: Methods: Theory and Modeling*; Andreoni, W., Yip, S., Eds.; Springer International Publishing: Cham, 2020; pp 621–634.
- (39) Maragliano, L.; Vanden-Eijnden, E. A Temperature Accelerated Method for Sampling Free Energy and Determining Reaction Pathways in Rare Events Simulations. *Chem. Phys. Lett.* **2006**, *426*, 168.
- (40) Abrams, J. B.; Tuckerman, M. E. Efficient and Direct Generation of Multidimensional Free Energy Surfaces via Adiabatic Dynamics without Coordinate Transformations. *J. Phys. Chem. B* **2008**, *112*, 15742.
- (41) Rosso, L.; Mináry, P.; Zhu, Z.; Tuckerman, M. E. On the use of the adiabatic molecular dynamics technique in the calculation of free energy profiles. *J. Chem. Phys.* **2002**, *116*, 4389.
- (42) Rosso, L.; Abrams, J. B.; Tuckerman, M. E. Mapping the Backbone Dihedral Free-Energy Surfaces in Small Peptides in Solution Using Adiabatic Free-Energy Dynamics. *J. Phys. Chem. B* **2005**, *109*, 4162.

- (43) Chen, M.; Cuendet, M. A.; Tuckerman, M. E. Heating and Flooding: A Unified Approach for Rapid Generation of Free Energy Surfaces. *J. Chem. Phys.* **2012**, *137*, 024102.
- (44) Awasthi, S.; Nair, N. N. Exploring High Dimensional Free Energy Landscapes: Temperature Accelerated Sliced Sampling. *J. Chem. Phys.* **2017**, *146*, 094108.
- (45) Awasthi, S.; Gupta, S.; Tripathi, R.; Nair, N. N. Mechanism and Kinetics of Aztreonam Hydrolysis Catalyzed by Class-C  $\beta$ -Lactamase: A Temperature-Accelerated Sliced Sampling Study. *J. Phys. Chem. B* **2018**, *122*, 4299–4308.
- (46) Vithani, N.; Jagtap, P. K. A.; Verma, S. K.; Tripathi, R.; Awasthi, S.; Nair, N. N.; Prakash, B. Mechanism of  $Mg^{2+}$ -Accompanied Product Release in Sugar Nucleotidyltransferases. *Structure* **2018**, *26*, 459 – 466.
- (47) Sahoo, S. K.; Nair, N. N. Interfacing the Core-Shell or the Drude Polarizable Force Field With Car-Parrinello Molecular Dynamics for QM/MM Simulations. *Front Chem.* **2018**, *6*, 275.
- (48) Soniya, K.; Awasthi, S.; Nair, N. N.; Chandra, A. Transimination Reaction at the Active Site of Aspartate Aminotransferase: A Proton Hopping Mechanism through Pyridoxal 5'-Phosphate. *ACS Catal.* **2019**, *9*, 6276–6283.
- (49) Kapakayala, A.; Gupta, A.; Verma, S.; Nair, N. N. Free energy calculations of alanine tripeptide in explicit water using temperature accelerated sliced sampling. *J. Indian Chem. Soc.* **2019**, *96*, 875–882.
- (50) Bonomi, M.; Branduardi, D.; Bussi, G.; Camilloni, C.; Provasi, D.; Raiteri, P.; Donadio, D.; Marinelli, F.; Pietrucci, F.; Broaglia, R. A.; Parrinello, M. PLUMED: A portable plugin for free-energy calculations with molecular dynamics. *Comput. Phys. Commun.* **2009**, *180*, 1961.

- (51) Bonomi, M.; Barducci, A.; Parrinello, M. Reconstructing the Equilibrium Boltzmann Distribution from Well-tempered Metadynamics. *J. Comput. Chem.* **2009**, *30*, 1615.
- (52) Cuendet, M.; Tuckerman, M. Free Energy Reconstruction from Metadynamics or Adiabatic Free Energy Dynamics Simulations. *J. Chem. Theory Comput.* **2014**, *10*, 2975–2986.
- (53) Tiwary, P.; Parrinello, M. A Time-Independent Free Energy Estimator for Metadynamics. *J. Phys. Chem. B* **2014**, *119*, 736.
- (54) Marinova, V.; Salvalaglio, M. Time-independent free energies from metadynamics via mean force integration. *J. Chem. Phys.* **2019**, *151*, 164115.
- (55) Giberti, F.; Cheng, B.; Tribello, G.; Ceriotti, M. Iterative Unbiasing of Quasi-Equilibrium Sampling. *J. Chem. Theory Comput.* **2020**, *16*, 100–107.
- (56) Comer, J.; Gumbart, J. C.; Hénin, J.; Lelièvre, T.; Pohorille, A.; Chipot, C. The Adaptive Biasing Force Method: Everything You Always Wanted To Know but Were Afraid To Ask. *J. Phys. Chem. B* **2015**, *119*, 1129.
- (57) Samanta, A.; Chen, M.; Yu, T.-Q.; Tuckerman, M.; E, W. Sampling saddle points on a free energy surface. *J. Chem. Phys.* **2014**, *140*, 164109.
- (58) Chen, M.; Yu, T.-Q.; Tuckerman, M. E. Locating Landmarks on High-Dimensional Free Energy Surfaces. *Proc. Natl. Acad. Sci.* **2015**, *112*, 3235.
- (59) Maier, J. A.; Martinez, C.; Kasavajhala, K.; Wickstrom, L.; Hauser, K. E.; Simmerling, C. ff14SB: Improving the Accuracy of Protein Side Chain and Backbone Parameters from ff99SB. *J. Chem. Theory Comput.* **2015**, *11*, 3696.



- (60) Tribello, G. A.; Bonomi, M.; Branduardi, D.; Camilloni, C.; Bussi, G. PLUMED 2: New feathers for an old bird. *Comput. Phys. Commun.* **2014**, *185*, 604 – 613.
- (61) Schneider, E.; Dai, L.; Topper, R. Q.; Drechsel-Grau, C.; Tuckerman, M. E. Stochastic Neural Network Approach for Learning High-Dimensional Free Energy Surfaces. *Phys. Rev. Lett.* **2017**, *119*, 150601.
- (62) Bonati, L.; Zhang, Y.-Y.; Parrinello, M. Neural networks-based variationally enhanced sampling. *Proc. Nat. Acad. Sci.* **2019**, *116*, 17641–17647.
- (63) Wehmeyer, C.; Noé, F. Time-lagged autoencoders: Deep learning of slow collective variables for molecular kinetics. *J. Chem. Phys.* **2018**, *148*, 241703.
- (64) Ribeiro, J. M. L.; Bravo, P.; Wang, Y.; Tiwary, P. Reweighted autoencoded variational Bayes for enhanced sampling (RAVE). *J. Chem. Phys.* **2018**, *149*, 072301.
- (65) Chen, W.; Ferguson, A. L. Molecular enhanced sampling with autoencoders: On-the-fly collective variable discovery and accelerated free energy landscape exploration. *J. Comput. Chem.* **2018**, *39*, 2079–2102.
- (66) Sultan, M. M.; Pande, V. S. Automated design of collective variables using supervised machine learning. *J. Chem. Phys.* **2018**, *149*, 094106.
- (67) Cendagorta, J. R.; Tolpin, J.; Schneider, E.; Topper, R. Q.; Tuckerman, M. E. Comparison of the Performance of Machine Learning Models in Representing High-Dimensional Free Energy Surfaces and Generating Observables. *J. Phys. Chem. B* **2020**, *124*, 3647–3660.